Optics and Lasers in Engineering 137 (2021) 106334

Contents lists available at ScienceDirect

Optics and Lasers in Engineering

journal homepage: www.elsevier.com/locate/optlaseng

Effects of immersion depth on the dynamics of cavitation bubbles generated during ns laser ablation of submerged targets

Jiangyou Long[a,b,*], Matthew H. Eliceiri[b], Yuexing Ouyang[a], Yongkang Zhang[a], Xiaozhu Xie[a,c], Costas P. Grigoropoulos[b,*]

[a] Laser Micro/Nano Processing Lab, School of Electromechanical Engineering, Guangdong University of Technology, Guangzhou 510006, P.R. China
[b] Laser Thermal Laboratory, Department of Mechanical Engineering, University of California, Berkeley, CA 94720-1740, USA
[c] State Key Laboratory of Precision Electronic Manufacturing Technology and Equipment, Guangdong University of Technology, Guangzhou 510006, P.R. China

ARTICLE INFO

Keywords:
Time-resolved imaging
Shadowgraphy
Laser ablation
Cavitation
Underwater laser micromachining
Laser shock peening

ABSTRACT

On laser shock peening and underwater laser micromachining, previous studies have shown that the immersion depth of the sample significantly affects laser ablation of submerged targets; however, the underlying mechanisms are still obscure. In this work, we observe and study the formation, growth, and collapse of cavitation bubbles generated during nanosecond laser ablation of submerged titanium targets that are exposed at various immersion depths utilizing a stroboscopic shadowgraphy system. Our results show that the initial laser absorption and cavitation bubble formation after the laser incidence are not affected by the immersion depth. Nevertheless, when the immersion depth is less than the maximum radius of the generated cavitation bubble, the bubble shrinks asymmetrically during the collapse stage. Thus, the cavitation bubble is not fully compressed at the maximum implosion, and phenomena related to the violent implosive collapse, e.g., the second etching effect and the emission of strong shockwaves, are absent. We also propose a strategy to estimate the maximum radius of the laser-induced cavitation bubble, which helps to determine the optimal liquid depth for related engineering applications. Our results provide succinct explanations for the effects of immersion depth on pulsed laser ablation of submerged targets, which are important steps toward a deeper understanding of laser-materials' interactions in liquid environments.

1. Introduction

Several important phenomena occur both during and after pulsed laser ablation of submerged targets. First, a strong shockwave propagating through the target is generated. A method known as laser shock peening is proposed utilizing this mechanism, wherein a layer of the sample surface is ablated in water by high-energy laser pulses to generate the shockwave. The emitted shockwave induces compressive residual stress on the sample surface, which significantly improves the fatigue strength of the component [1,2]. Second, an explosive cavitation bubble forms during the ablation, which enables fast nucleation and growth of fine nanoparticles inside the bubble [3,4]. Numerous compositions and morphologies of nanomaterials that are difficult to prepare via conventional approaches can be easily prepared by laser ablation of bulk materials in liquid environments [5,6]. Finally, during or after the collapse of a laser-induced cavitation bubble, a high-speed fluid microjet directed towards the target surface forms [7], which helps with the removal of surface debris generated during the laser ablation. In addition to the suppressed thermal damage, underwater laser machining has shown benefits for fine cutting, grooving, and drilling [8–11].

Previous studies on applications related to underwater laser ablation have highlighted the importance of the sample's immersion depth (H): it affects both the amplitude of laser-induced shockwaves and the ablation efficiency [12–17]. Takata et al. [12] investigated the effect of H on the impact force of laser-induced shockwaves generated during laser shock peening, which was evaluated through the detected acoustic emission waveforms. The results showed that the impact of shockwaves can be detected after both laser incidence and bubble collapse; the former only slightly changes, but the latter notably increases with increasing H from 1 to 4 mm. This result is well consistent with that of Kadhim et al. [13], which states that the surface microhardness of the laser-processed samples dramatically increases with increasing H from 1 to 3 mm in laser shock peening. In another study [17], an optimal H of 3 mm was recorded for the maximum efficiency of underwater laser drilling. Numerous studies have tried to clarify the effects of H on underwater laser ablation, but clear physical mechanisms and convincing experimental supports are still lacking. For example, high-speed images with a frame

* Corresponding authors.
E-mail addresses: longjy@gdut.edu.cn (J. Long), cgrigoro@berkeley.edu (C.P. Grigoropoulos).

https://doi.org/10.1016/j.optlaseng.2020.106334
Received 8 May 2020; Received in revised form 7 August 2020; Accepted 10 August 2020

Nomenclature

H	Sample's immersion depth
t	Delay time between the ablation and imaging pulses
F	Laser fluence
E	Laser pulse energy
R	Cavitation bubble radius
E_0	The energy stored in the liquid-bubble system
P_B	Pressure within the bubble
P_{max}	The pressure maximum in the surrounding liquid
a	A dimensionless constant chiefly depends on E
β	Energy conversion efficiency
D	Thermal penetration depth
b	Thermal diffusivity
τ	Thermal diffusion time
R_{max}	Maximum bubble radius during the evolution
T	The lifetime of the cavitation bubble
E_B	The energy of the cavitation bubble
h	Bubble height
w	Bubble width
P_∞	Liquid pressure far from the bubble
ΔP	The pressure difference inside and outside the cavitation bubble when it grows to its maximum size
ρ	Liquid density
μ	Dynamic viscosity
σ	Surface tension
P_0	Bubble pressure at a point of reference
R_0	The bubble radius when $P_B = P_0$
γ	Heat capacity ratio of the gas inside the bubble
c	The Vander Waals hardcore
R_{t800}	R at $t = 800$ ns when $F = 29.8$ J/cm^2 and $H = 4$ mm
P_{t800}	P_B at $t = 800$ ns when $F = 29.8$ J/cm^2 and $H = 4$ mm
We	Weber number
Re	Reynolds number
R_c	R at the instant of collapse
P_c	P_B at the instant of collapse
V	The volume of the residual bubble layer at the instant of collapse
δ	Average ablation rate

rate of 220,000 fps during underwater laser ablation were acquired by Takata et al. [12]. They observed that the generated cavitation bubble contacted the liquid-air interface during the expansion stage when using a thin water layer. However, they did not explain the effect of this phenomenon on the subsequent processes. Nguyen et al. [18] investigated the effects of immersion depth on the dynamics of laser-induced cavitation bubbles using a high-speed laser stroboscopic videography system in the photoelasticity mode. They found that the lifetime of a laser-induced cavitation bubble shortened as H decreased, but they did not explain the underlying mechanisms.

Although laser ablation has been extensively studied experimentally and theoretically, the production of experimental results of the transient localized state of laser-irradiated areas remains a challenge [19–22]. In this work, we aim to elucidate the effects of H on underwater laser ablation by observing and studying the evolution of laser-induced cavitation bubbles generated at different values of H. High-resolution nanosecond-resolved images of laser-induced cavitation bubbles provide vital information regarding the transient states of laser-irradiated areas, which are irreplaceable evidence to explain the underlying mechanisms. Our results demonstrated that when 0.5 mm $\leq H \leq$ 4 mm, its effects on the initial laser absorption and bubble formation become negligible. Nevertheless, the laser-induced cavitation bubble contacts the water-air interface during the expansion stage when using a thin water layer, which results in an asymmetric shrinkage of the bubble during the subsequent collapse stage. The consequence of this mechanism is that phenomena related to the intense implosive collapse are absent. The present work illuminates how H affects laser ablation of submerged targets and provides a coherent framework to comprehend, model, and test laser-materials' interactions in liquid environments.

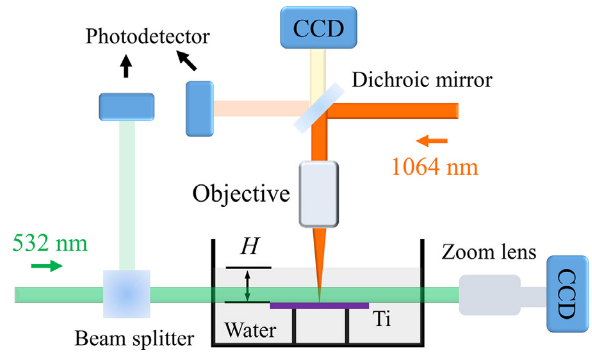

Fig. 1. Schematic of the experimental setup.

2. Materials and method

The experimental setup has been previously described in detail [23]. As shown in Fig. 1, a 1064 nm and a 532 nm Nd: YAG nanosecond (ns) laser are employed for ablation and imaging, respectively. The focused 1064 nm laser beam, with a diameter of 48 μm and a pulse width (FWHM) of 20 ns, irradiates the polished titanium (Ti) sample (Ti > 99.5 wt.%, size: 15 × 6 mm, thickness: 1 mm) that is immersed in water with H varying from 0.5 to 4 mm. The expanded 532 nm laser beam with a pulse width of 4 ns passes parallel to the surface of the Ti target, providing a shadowgraph image on a CCD camera coupled with a zoom lens system. The two laser beams are triggered by a delay generator, and their exact delay time (t), i.e., the time interval between two pulses' rising edge median (half-maximum), is confirmed by using two photodetectors connected to an oscilloscope. All components are selected to ensure a high temporal resolution. The obtained images are processed by a Sobel operator to emphasize edges, and then the shockwaves and the cavitation bubbles are circularly fitted to measure their radii. The laser ablation rate is calculated by measuring the volume of laser-ablated pits through a three-dimensional (3D) laser scanning microscope (OLS4100, Olympus). The averages of five laser-ablated pits are reported in the text. The morphology of laser-ablated areas is observed using a scanning electron microscope (SEM, FEI Quanta 3D FEG).

3. Results and discussion

3.1. Formation of shockwaves and cavitation bubbles after laser incidences

The evolution of shockwaves and cavitation bubbles after laser incidences under a typical laser fluence (F) are demonstrated in Fig. 2a and b. The profiles of shockwaves and cavitation bubbles can be distinguished after less than 20 ns. Afterward, the emitted shockwave propagates at a nearly constant speed. Previously, when using 60 mJ laser pulses, it was found that the speed of emitted shockwave decayed within the initial 300 ns and then quickly reached a constant [24]. However, since the maximum pulse energy used in this work is only 1.02 mJ, the initial decay phase may not noticeable. When F = 68.5 J/cm^2, the average propagation speed of the emitted shockwaves within the initial 200 ns (s) is 1625 m/s at H = 4 mm and 1617 m/s at H = 0.5 mm. These values decrease to 1595 m/s (H = 4 mm) and 1597 m/s (H = 0.5 mm) when F declines to 29.8 J/cm^2. The

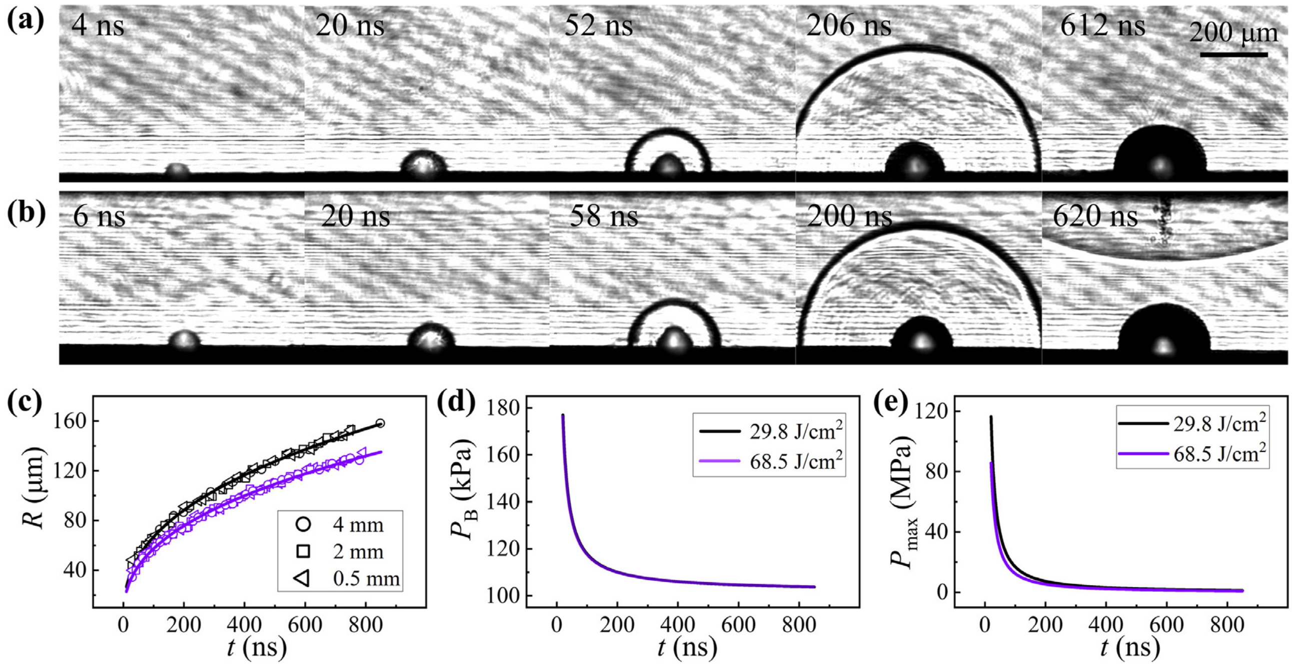

Fig. 2. (a, b) Shadowgraph images of shockwaves and cavitation bubbles generated after laser shots. Inserted text: t. Laser fluence (F): 68.5 J/cm^2. H: (a) 4 mm, (b) 0.5 mm. (c) Measured bubble radius (R). Black symbols: F = 68.5 J/cm^2; Violet symbols: F = 29.8 J/cm^2. Solid lines: Curves fitted by Eq. (1) when H = 4 mm. (d, e) Calculated bubble pressure (P_B) and maximum pressure in the surrounding liquid (P_{max}) as a function of t when H = 4 mm, respectively. The fitted curves of R and the calculated profiles of P_B and P_{max} under other values of H are similar to these demonstrated and are thus not shown in the figures.

speed of emitted shockwaves after laser incidences is primarily dependent on F, and the effect of H on it is very limited and lies within the range of measurement error. Furthermore, when H = 0.5 mm, the emitted shockwave bounces off the liquid-air interface, triggering the injection of microbubbles near the interface (t = 620 ns), as shown in Fig. 2b. This phenomenon can also be observed when H = 4 mm, but occurs much later because of the higher water-air interface. The energy released during underwater laser ablation is partly distributed in the shockwaves [25]. However, the shockwaves dissipate in the liquid and do not influence the subsequent processes. Consequently, our analysis will focus on the dynamics of laser-induced cavitation bubbles.

Fig. 2c summarizes the early radii variation of laser-induced cavitation bubbles, starting from t ~20 ns when the profiles of shockwaves and bubbles are distinguishable. The early variation of bubble radius (R) with t (20 ns < t < 800 ns) is dominated by F and are almost identical when H changes from 0.5 to 4 mm. As discussed in detail in our earlier study [23], laser ablation of submerged targets can be regarded as an intense point explosion underwater and the early fluid displacement outside the cavitation bubble is a hemispherical self-similar motion. Thus, the early variation of bubble radius (R) with t can be described by:

$$R = at^{2/5} \tag{1}$$

When assuming the released energy during laser ablation that drives the formation of cavitation bubbles (E_0) is totally converted into the kinetic energy of surrounding fluid, we get $a = (25E_0/4\pi\rho)^{1/5}$ with ρ being the liquid density [23]. We observed the changes of R with t under various F and H and then obtained the values of a and E_0 via fitting the corresponding R-t curves by Eq. (1), as demonstrated in Fig. 2c. Furthermore, the pressure within the bubble (P_B) and pressure maximum in the surrounding liquid (P_{max}) can be expressed as follows:

$$P_B = P_\infty + \frac{4\mu}{R}\frac{dR}{dt} + \frac{2\sigma}{R} \tag{2}$$

$$P_{max} - P_\infty = \frac{3}{50}4^{-1/3}\rho a^2 t^{-6/5} \tag{3}$$

where μ and σ are the dynamic viscosity and surface tension of the liquid (0.85 mPa·s and 72.0 mN/m for water), respectively; P_∞ represents the liquid pressure far from the bubble (~0.101 MPa).

When F = 68.5 J/cm^2, which corresponds to the laser pulse energy E = 620 μJ, the obtained E_0 are 67.3, 67.1, and 66.5 μJ at H = 0.5, 2, and 4 mm, respectively. When E decreases to 270 μJ, the above values of E_0 decrease to 31.9, 31.2, and 31.0 μJ, respectively. In both instances, ~10% – 11% of the laser pulse energy was converted into the bubble–liquid energy after the laser ablation and the conversion efficiency ($\beta = E_0/E$) was not affected by H.

The calculated P_B and P_{max} as a function of t when H = 4 mm, starting from t = 20 ns, are conveyed in Fig. 2d and e. Both P_B and P_{max} decay rapidly with t. When F increases from 29.8 to 68.5 J/cm^2, P_B and P_{max} at t = 20 ns increase from 176.3 kPa and 85.7 MPa to 177.0 kPa and 116.5 MPa, respectively. For an intense point explosion underwater, the released energy during the explosion mainly exists in the fluid around the cavitation bubble in the early stage; thus, P_B only changes slightly while the P_{max} greatly increases with increasing F.

In summary, the propagation of emitted shockwaves and the early evolution of generated cavitation bubbles after laser incidences are almost identical when H changes from 0.5 to 4 mm. Consequently, we are able to conclude that H does not affect both laser absorption and bubble formation after the laser incidence. If we further analyze the related details, then we find that the drawn conclusion is rational. First, the laser peak power intensity in this study is ~10^9 W/cm^2, not high enough to trigger the nonlinear absorption of light in a transparent material [26]. The absorption coefficient of pure water at 1064 nm is 0.144 cm^{-1}, which corresponds to a transmittance of 99.3% and 94.4% when H is 0.5 and 4 mm, respectively [27]. The effect of H on the laser energy arriving at the target surface is very limited. Second, from the perspective of thermal diffusion, the thermal penetration depth (D) can be estimated by $D \sim \sqrt{b\tau}$, where b and τ are the thermal diffusivity (~0.14 × 10^{-6} m^2/s for liquid water) and thermal diffusion time, respectively [28,29]. D is just hundreds of nanometers after 50 ns of the laser incidence; an amount significantly less than the minimum H = 0.5 mm employed in

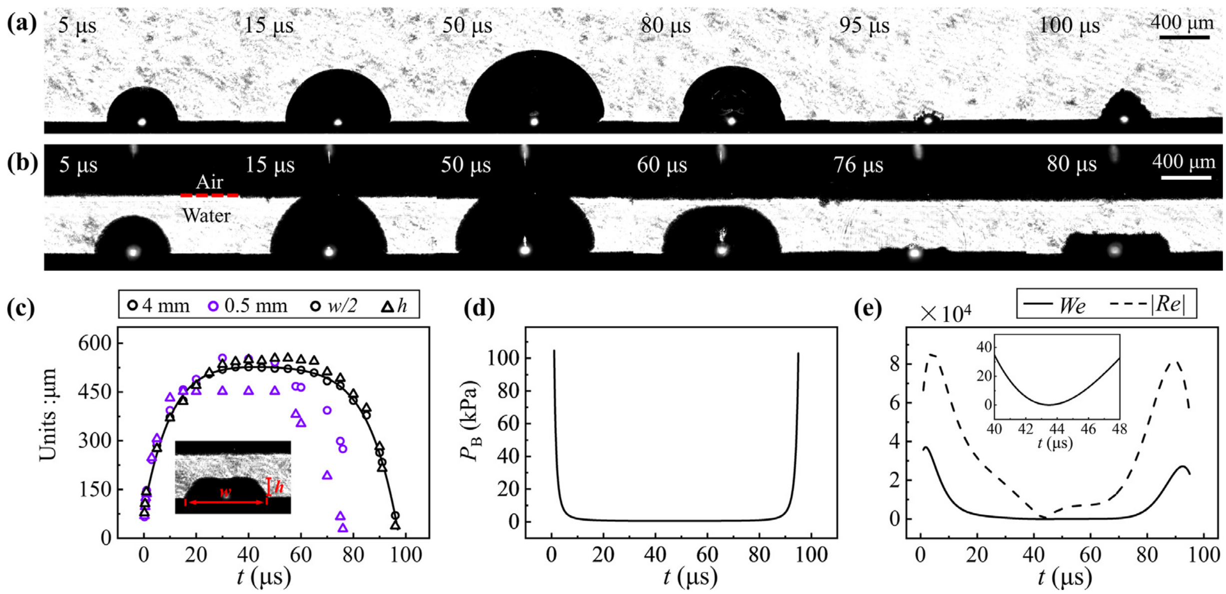

Fig. 3. (a, b) Evolution of laser-induced cavitation bubbles. *F*: 29.8 J/cm^2. *H*: (a) 4 mm, (b) 0.5 mm. (c) Variations of bubble height (h) and half of the bubble width ($w/2$) with t. Solid line: the fitted curve using seventh order polynomial regressions. (d, e) Variations of P_B, We, and $|Re|$ with t (1 μs $\le t \le$ 94 μs, correspondingly R > 130 μm) when H = 4 mm.

our experiments. Consequently, the effect of H on thermal diffusion can also be ignored.

3.2. Growth and collapse of laser-induced cavitation bubbles

Further, we observed the growth and collapse of laser-induced cavitation bubbles. The evolution of cavitation bubbles generated under a typical F of 29.8 J/cm^2 is described and analyzed here in detail. After the initial rapid expansion, the laser-induced cavitation bubble further expands to a maximum size and then shrinks and collapses, emitting a new shockwave. The cavitation bubble then rebounds, as shown in Fig. 3a. When H = 4 mm, the maximum radius (R_{max}) and the lifetime (T) of the cavitation bubble from the origination to the first collapse are 526 μm and 96 μs, respectively. In the absence of surface tension and gas content, the energy of cavitation bubble (E_B) can be estimated by [7,30]:

$$E_B = (2/3)\pi R_{max}^3(\Delta P), \tag{4}$$

$$T/2 = 0.915 R_{max}(\rho/\Delta P)^{1/2}, \tag{5}$$

where ΔP represents the pressure difference inside and outside the cavitation bubble when it grows to its maximum size. The calculated E_B is 30.6 μJ, which well corresponds to the obtained E_0 in Section 3.1 (31.0 μJ). When the cavitation bubble is static as it grows to its maximum size, the kinetic energy of the surrounding liquid completely transforms into the potential energy of the bubble, and thus $E_B \sim E_0$.

When H decreases to 0.5 mm, the expanding bubble contacts the water-air interface after ~15 μs. The upper side of the bubble is then pinned to the water-air interface, and the bubble further expands in the horizontal direction, as shown in Fig. 3b. After ~60 μs, the upper side of the bubble detaches from the interface and the bubble shrinks rapidly, collapsing at t ~76 μs. The lifetime of the laser-induced cavitation bubbles is shortened as demonstrated in the previous report [18].

The changes in the height (h) and half of the width ($w/2$) of the bubbles with t are summarized in Fig. 3c. The laser-induced cavitation bubbles are hemispherical when H = 4 mm, as the changes in h and $w/2$ follow a very similar trajectory. The early bubble expansion before the contact is also hemispherical when H decreases to 0.5 mm, however, the bubble lost its symmetry and shrinks much faster in the vertical direction after detaching from the interface. The maximum $w/2$ reached at H = 0.5 and 4 mm are similar, i.e., the contact between the bubble wall and the liquid-air interface does not affect the horizontal expansion of the bubble. Based on the observed bubble evolution when H = 4 mm, we calculated the pressure changes within the bubble during the expansion and shrinkage, which helps to explain the asymmetrical shrinkage of cavitation bubbles when H = 0.5 mm.

The bubble dynamics can be analytically described using the Rayleigh-Plesset (RP) equation when the speed of the bubble wall, $\dot{R}$, is small compared to the speed of sound in the gas [31]:

$$R\ddot{R} + \frac{3}{2}\dot{R}^2 = \frac{1}{\rho}\left[P_B - P_\infty - \frac{2\sigma}{R} - \frac{4\mu\dot{R}}{R}\right] \tag{6}$$

Although the RP equation fails in the late stage of implosive collapse, it well describes the bubble dynamics during the expansion and shrinkage stages. In the absence of any significant thermal effects and neglecting mass transfer through the bubble, the gas pressure within the bubble can be determined by using an adiabatic equation of state, including the effect of the Vander Waals hardcore "c" [32]:

$$P_B = \frac{P_0 {R_0}^{3\gamma}}{(R^3 - c^3)^\gamma} \tag{7}$$

where γ is the heat capacity ratio of the gas inside the bubble, and P_0 and R_0 are the pressure and radius of the bubble at a point of reference, respectively. The value of c is very small, usually several hundreds of nanometers [33]. Thus, it can be neglected when $R >> 1$ μm. Extensive efforts have been made to estimate the pressure changes within the bubble based on Eqs. (6) and (7) [34,35]. Nevertheless, obtaining the status of a reference point, i.e., the values of P_0 and R_0, is difficult. Herein, as the early variations of P_B with t have been calculated in Fig. 2, the radius and pressure of the bubble at t = 800 ns (R_{t800} = 153.8 μm and P_{t800} = 103.9 kPa) can be employed as R_0 and P_0, respectively. Thus, we propose a simplified method to estimate P_B during the expansion and shrinkage stages. First, we employed the $w/2$ as the bubble radius R, and its evolution was fitted using seventh order polynomial regressions, as shown in Fig. 3c. Then, P_B is calculated by:

$$P_B = P_t800\left(R_t800/R\right)^{3\gamma} (\text{for } R > 100\ \mu\text{m}) \tag{8}$$

The main gas composition inside the bubble is probably water vapor, whose γ is 1.33 [33,36]. Moreover, the effect of the laser-ablated mate-

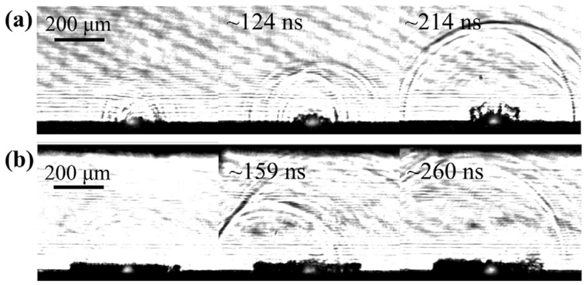

Fig. 4. Shadowgraph images after the collapse of laser-induced cavitation bubbles. F: 29.8 J/cm^2. H: (a) 4 mm, (b) 0.5 mm. Inserted text: t_i.

rials inside the bubble, which mainly exist in the form of nanoparticles, should be considered. In the case of gas dynamics, the medium with a great number of particles behaves as a gas that has less γ than pure gas [37]. Thus, γ is assumed to be 1.25 here. The calculated P_B as a function of t is shown in Fig. 3d. P_B decays rapidly to ~2.00 kPa after ~10 μs. Afterward, it gradually decreases and reaches a minimum of ~0.54 kPa at t ~43 μs. P_B then starts to increase as the bubble shrinks, and this increase becomes sharp after ~90 μs. Evidently, the pressure within the bubble is very low during the expansion stage, especially when the bubble grows to a size that is almost its maximum size.

According to the evolution of $P_{B,}$ we propose a mechanism to explain the asymmetric collapse of cavitation bubbles when employing thin water layers. When $H < R_{max}$, the expanding bubble contacts the liquid-air interface, which results in the formation of a raised interface. These raised aspheric interfaces, which have been observed in Nguyen et al.'s works [18,38], lead to increased surface tension in the vertical direction. As the pressure within the bubble is very low when it reaches its maximum size, the increased surface tension due to the raised interface causes a much higher acceleration in the vertical direction when the bubble detaches from the interface. Consequently, the bubble loses its symmetry and shrinks much faster in the vertical direction. This mechanism is well supported when we compare the relative contribution of inertial force, viscous force, and surface tension to the dynamics of cavitation bubbles. The changes in the Weber number ($We = \rho \dot{R}^2 R/\sigma$), which represents the ratio of inertial force to surface tension, and the absolute value of Reynolds number ($|Re| = |\rho \dot{R} R/\mu|$), which expresses the ratio of inertial force to viscous force, with t are depicted in Fig. 3e. During the evolution of cavitation bubbles, the viscous force can be neglected as $|Re| >> 10^3$ during most of the process. Although $We > 10^2$ for most of the process, it decreases to a very small value as the bubble grows to size near its maximum size, as shown in the inset of Fig. 3e. Namely, the effect of surface tension becomes more dominant when the bubble grows to its maximum size.

The asymmetric shrinkage of cavitation bubbles further affects the late stage of implosive collapse. To clarify this remark, we observed the instant of collapse of cavitation bubbles under high magnification. As only one photograph at a designed t can be acquired in one experiment and the instant of collapse slightly changes in every experiment (~1–2 μs), we acquired hundreds of images around the instant of collapse and selected among them for analysis those capturing shockwaves. The time interval between the captured images and the instant of collapse (t_i) is estimated based on the position of emitted shockwaves: $t_i = R_s/s$, where R_s is the radius of the observed shockwave.

Fig. 4 illustrates bubble evolution after the instant of collapse. The first figures in Fig. 4a and b are considered as the instant of collapse as the shockwaves are not fully emitted. Traces of multiple shock fronts can be found after the collapse. We increase the image brightness until only one shock front can be identified, which is employed to calculate the t_i here. When H = 4 mm, the cavitation bubble is compressed to an invisible size during the collapse and then expands rapidly to $w/2$ ~76 μm after ~214 ns, as shown in Fig. 4a. However, under the same F, a flat residual bubble layer with $w/2$ ~208 μm and h ~28 μm can be observed at the instant of collapse when H = 0.5 mm, as shown in Fig. 4b. This residual bubble layer expands slowly after the collapse, reaching $w/2$ ~227 μm and h ~36 μm after ~260 ns. The formation of the flat residual bubble layer may be attributed to two causes. First, the contact between the bubble and water-air interface may lead to an increase in gaseous substances inside the bubble, which hinders the implosive collapse of the bubble. More importantly, the cavitation bubbles shrink much faster in the vertical direction than in the horizontal direction, which results in an insufficient compression of the cavitation bubble at the maximum implosion during the collapse.

The energy of cavitation bubbles is stored in the liquid/bubble system during the growth stage and is focused and released during the implosive collapse. It is this focusing of energy in both space and time that results in most of the remarkable effects of cavitation [39]. Consequently, we believe that the different collapse process is key to clarify the role of H in the laser ablation of submerged targets. Due to the great complexity of bubble collapse, e.g., the thermal effects are not neglectable, the final stages of collapse may involve such high velocities that the assumption of liquid incompressibility is no longer appropriate, and a collapsing bubble loses its spherical symmetry [31,40], there is no simple theory for describing the bubble collapse. Therefore, we only roughly compare the pressure difference within the bubbles at the instant of collapse at different H based on Eq. (7), neglecting the effect of c. If we assume an identical initial state of the cavitation bubble containing few noble gasses whose γ = 1.66, the pressure within the cavitation bubbles at the instant of collapse (P_c) would be proportional to $1/R_c^{4.98}$ where R_c represents the minimum bubble radius during the collapse. When H = 4 mm, we assume that the R_c is 5 μm, which is approximately the resolution limit for our imaging system; when H = 0.5 mm, R_c is approximated by the volume of the flat residual bubble (V), assuming a hollow cylindrical shape with internal radius $w/4$ and external radius $w/2$ [18], and thus we have $V = 3\pi h w^2/16 = 2\pi R_c^3/3$. The estimated R_c when H = 0.5 mm approximates 110 μm. The calculated Pc when H = 4 mm would be six orders of magnitude higher compared to that when H = 0.5 mm. It is noteworthy that this comparison is very simplified, which just used to show the huge pressure difference within the bubbles that could be reached when the minimum bubble size differs.

Our results clearly explain the effects of H on laser ablation of submerged targets. When $H > R_{max}$, the intense compression of cavitation bubbles during the implosive collapse triggers a dramatic increase in localized temperature and pressure. The temperature and pressure inside the bubble can be high enough to cause melting or evaporation of the substrate. Thus, when combined with the impact of high-speed microjets produced by collapsing cavitation bubbles [7], it drives a second etching (cavitation erosion) and emits a strong shockwave. In contrast, when $H < R_{max}$, the expanding cavitation bubble contacts the water-air interface, which results in an asymmetric shrinkage and an insufficient compression of the cavitation bubble. As a result, the second etching effect is absent and the emitted shockwave after bubble collapse is much weaker. Our proposed mechanisms clearly explain the phenomena observed in Takata et al.'s work, i.e., the impact force after the bubble collapse during laser shock peening remarkedly increases when H increases from 1 to 4 mm [12].

3.3. Ablation rate and morphology of ablated areas

To further verify our proposed mechanism, we measured the laser ablation rate (δ) on Ti specimens immersed in water at various H. As shown in Fig. 5a, the value of δ is much higher in air than in water because of the enhanced cooling effect of laser-irradiated areas in the water environment. Furthermore, H also affects δ. The values of δ when H = 4 and 2 mm are quite similar, but there is a notable decrease when H decreases to 0.5 mm. This decrease becomes more obvious when employing moderate values of F. R_{max} increases with increasing F. In our study, the observed R_{max} is 710 and 850 μm when F is 68.5 and 112.7 J/cm^2,

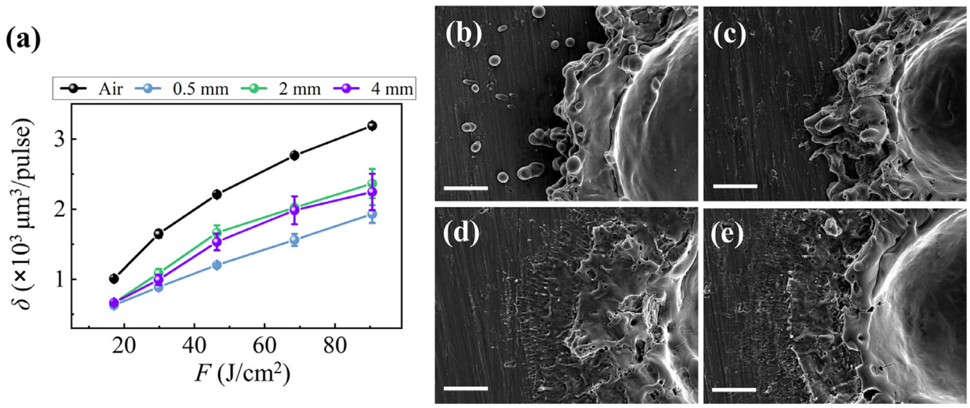

Fig. 5. (a) Average ablation rate (δ) in air and in water at various H after 20 laser shots under a laser repetition rate of 0.2 Hz. (b-e) SEM images of laser-ablated areas; (b) in air and (c-e) in water when H is 0.5, 2, and 4 mm, respectively. F: 68.4 J/cm^2. Scale bars: 10 μm.

respectively, as shown in Fig. 6. Consequently, for F employed here, a 2-mm thick water layer is enough to avoid the contact between the bubble and water-air interface, and it enables the violent implosive collapse and the effective second etching. With increasing F, the effect of second etching becomes increasingly obvious and the δ noticeably increases when H increases from 0.5 to 2 mm. However, we noticed that the water layer tends to flow after laser shots under high F, which increased the fluctuation of δ, as shown in Fig. 5a. Consequently, the difference in δ at different H decreases when increasing the F to 112.7 J/cm^2. H affects not only the ablation rate but also the morphology around the laser-ablated areas, as shown in Fig. 5b–e. When $H = 0.5$ mm, the morphology around the laser-ablated areas is similar to that in air. As H increases to ≥2 mm, thermal damage around the ablated pits can be observed, which is probably a side effect of the second etching effect.

3.4. Estimating the maximum bubble radius

Our results highlighted the importance of R_{max} in applications related to laser ablation of submerged targets. It would be meaningful to provide a simple method for estimating the value of R_{max} for engineering applications. R_{max} can be obtained by Eq. (4) when the values of E_B and ΔP are both known. The pressure within the bubble is very low when the bubble grows to its maximum size, and thus we get $\Delta P \sim P_\infty$. The value of E_B depends on the E and the energy conversion efficiency β: $E_B = E \times \beta$. β is a comprehensive coefficient related to both the laser parameters, e.g., wavelength and pulse duration, and the target properties. For instance, the β reached 20% when the target was covered by an absorptive coating [41]. Nevertheless, according to our results, the value of β does not obviously depend on E within a certain range, and thus it can be confirmed by observing the laser-induced cavitation bubbles under some typical E. Both Eq. (1) and (3) and (4) can be employed to determine the values of E_B (or E_0) and then β under typical E. In our study, β ~11% when 0.27 mJ ≤ E ≤ 1.02 mJ. Fig. 6 shows the calculated R_{max} [$R_{max} = (3E\beta/2\pi P_\infty)^{1/3}$] as a function of E, which corresponds well to the observed values.

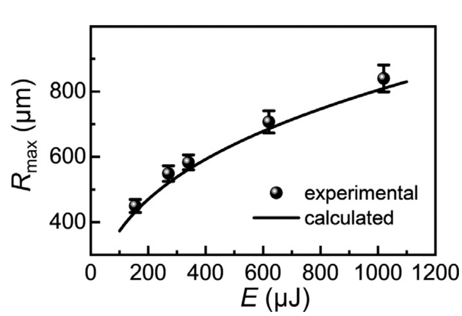

Fig. 6. Measured and calculated maximum bubble radii under various laser pulse energy.

4. Conclusions

We presented a comprehensive analysis of the dynamics of cavitation bubbles generated during pulsed laser ablation of submerged Ti targets by employing a high-resolution stroboscopic shadowgraphy system. The effects of H on the initial bubble evolution and the subsequent bubble growth and collapse were investigated. The main conclusions are as follow:

1) The speed of the emitted shockwaves and early bubble evolution just after the laser incidence are chiefly dependent on F, and the effects of H on them are ignorable when 0.5 mm ≤ H ≤ 4 mm.
2) When $H < R_{max}$, the expanding cavitation bubble contacted the liquid-air interface during the expansion stage, which results in the asymmetric shrinkage of the cavitation bubble during the subsequent shrinkage stage.
3) Further observations of the instant of collapse prove that the asymmetric shrinkage leads to insufficient compression of the cavitation bubble during the collapse. Consequently, phenomena related to the intense collapse, e.g., second etching effect and strong shockwaves emission, are absent when using thin water layers.

Our results well explain many phenomena observed in previous studies and provide insight into applications related to laser ablation of submerged targets, e.g., underwater laser micromachining and laser shock peening. In general, choosing an $H \geq 2R_{max}$ can ensure the intense implosive collapse of laser-induced cavitation bubbles, which results in a higher ablation rate and a double shock peening effect; however, the potential side effects may deteriorate the surface quality around the laser-ablated areas.

It is noteworthy that the laser spot size and the maximum laser pulse energy used in this work are 48 μm and 1.02 mJ, respectively, which corresponds well to the parameters used in underwater laser micromachining but are much smaller than those used in laser shock peening and forming. It would be fruitful to further verify whether our models and conclusions work under various parameter ranges, which we expect to explore in future work.

Declaration of Competing Interest

The authors declare that they have no known competing financial interests or personal relationships that could have appeared to influence the work reported in this paper.

CRediT authorship contribution statement

Jiangyou Long: Conceptualization, Methodology, Formal analysis, Investigation, Writing - original draft. **Matthew H. Eliceiri:** Methodology, Resources, Writing - review & editing. **Yuexing Ouyang:** Resources. **Yongkang Zhang:** Funding acquisition. **Xiaozhu Xie:** Funding acquisition. **Costas P. Grigoropoulos:** Supervision, Funding acquisition, Project administration, Writing - review & editing.

Acknowledgments

This work was conducted at the Laser Thermal Laboratory. The ablation rate measurement and SEM observation were carried out at the Marvell Nanofabrication Laboratory and the California Institute of Quantitative Bioscience (QB3) of UC Berkeley. Dr. Jiangyou Long acknowledges the funding support of National Natural Science Foundation of China (51805093, 51775117), National Key R&D Program of China (2018YFB1107700), Natural Science Foundation of Guangdong Province (2018A030310578), Ordinary University Characteristics Innovation Project of Guangdong Province (2017KTSCX056), Science and Technology Planning Project of Guangdong Province (2017B090911013), and the Chinese Scholars Council.

References

[1] Clauer AH. Laser shock peening, the path to production. Metals 2019;9:626. doi:10.3390/met9060626.
[2] Ding K, Ye L. Laser shock peening : performance and process simulations. Woodhead; 2006.
[3] Ibrahimkutty S, Wagener P, Menzel A, Plech A, Barcikowski S. Nanoparticle formation in a cavitation bubble after pulsed laser ablation in liquid studied with high time resolution small angle x-ray scattering. Appl Phys Lett 2012;101:103104. doi:10.1063/1.4750250.
[4] Letzel A, Gökce B, Wagener P, Ibrahimkutty S, Menzel A, Plech A, Barcikowski S. Size quenching during laser synthesis of colloids happens already in the vapor phase of the cavitation bubble. J Phys Chem C 2017;121:5356–65. doi:10.1021/acs.jpcc.6b12554.
[5] Yan Z, Chrisey DB. Pulsed laser ablation in liquid for micro-/nanostructure generation. J Photochem Photobiol C Photochem Rev 2012;13:204–23. doi:10.1016/j.jphotochemrev.2012.04.004.
[6] Zeng H, Du X-W, Singh SC, Kulinich SA, Yang S, He J, Cai W. Nanomaterials via laser ablation/irradiation in liquid: a review. Adv Funct Mater 2012;22:1333–53. doi:10.1002/adfm.201102295.
[7] Vogel A, Lauterborn W, Timm R. Optical and acoustic investigations of the dynamics of laser-produced cavitation bubbles near a solid boundary. J Fluid Mech 1989;206:299–338. doi:10.1017/S0022112089002314.
[8] Tsai CH, Li CC. Investigation of underwater laser drilling for brittle substrates. J Mater Process Technol 2009;209:2838–46. doi:10.1016/j.jmatprotec.2008.06.057.
[9] Mullick S, Madhukar YK, Roy S, Kumar S, Shukla DK, Nath AK. Development and parametric study of a water-jet assisted underwater laser cutting process. Int J Mach Tools Manuf 2013;68:48–55. doi:10.1016/j.ijmachtools.2013.01.005.
[10] Rashed CAA, Romoli L, Tantussi F, Fuso F, Burgener M, Cusanelli G, Allegrini M, Dini G. Water jet guided laser as an alternative to EDM for micro-drilling of fuel injector nozzles: a comparison of machined surfaces. J Manuf Process 2013;15:524–32. doi:10.1016/j.jmapro.2013.08.002.
[11] Kaakkunen JJJ, Silvennoinen M, Paivasaari K, Vahimaa P. Water-assisted femtosecond laser pulse ablation of high aspect ratio holes, in: phys. Procedia, Elsevier B.V. 2011:89–93. doi:10.1016/j.phpro.2011.03.110.
[12] Takata T, Enoki M, Chivavibul P, Matsui A, Kobayashi Y. Effect of confinement layer on laser ablation and cavitation bubble during laser shock peening. Mater Trans 2016;57:1776–83. doi:10.2320/matertrans.M2016150.
[13] Kadhim A, Salim ET, Fayadh SM, Al-Amiery AA, Kadhum AAH, Mohamad AB. Effect of multipath laser shock processing on microhardness, surface roughness, and wear resistance of 2024-T3 Al alloy. Sci World J 2014 2014. doi:10.1155/2014/490951.
[14] Kim D, Oh B, Lee H. Effect of liquid film on near-threshold laser ablation of a solid surface. Appl Surf Sci 2004;222:138–47. doi:10.1016/j.apsusc.2003.08.013.
[15] Kang HW, Welch AJ. Effect of liquid thickness on laser ablation efficiency. J Appl Phys 2007;101:083101. doi:10.1063/1.2715746.
[16] Al-Azawi MA, Bidin N, Ali AK, Hassoon KI, Abdullah M. Effect of liquid layer thickness on the ablation efficiency and the size-control of silver colloids prepared by pulsed laser ablation. Mod Appl Sci 2015;9:20–6. doi:10.5539/mas.v9n6p20.
[17] Krstulović N, Shannon S, Stefanuik R, Fanara C. Underwater-laser drilling of aluminum. Int J Adv Manuf Technol 2013;69:1765–73. doi:10.1007/s00170-013-5141-4.
[18] Nguyen TTP, Tanabe-Yamagishi R, Ito Y. Effects of liquid depth on the expansion and collapse of a hemispherical cavitation bubble induced in nanosecond pulsed laser ablation of a solid in liquid. Opt Lasers Eng 2020:126. doi:10.1016/j.optlaseng.2019.105937.
[19] Shih CY, Wu C, Shugaev MV, Zhigilei LV. Atomistic modeling of nanoparticle generation in short pulse laser ablation of thin metal films in water. J Colloid Interface Sci 2017;489:3–17. doi:10.1016/j.jcis.2016.10.029.
[20] Karim ET, Shugaev M, Wu C, Lin Z, Hainsey RF, Zhigilei LV. Atomistic simulation study of short pulse laser interactions with a metal target under conditions of spatial confinement by a transparent overlayer. J Appl Phys 2014:115. doi:10.1063/1.4872245.
[21] Shugaev MV, Wu C, Armbruster O, Naghilou A, Brouwer N, Ivanov DS, Derrien TJY, Bulgakova NM, Kautek W, Rethfeld B, Zhigilei LV. Fundamentals of ultrafast laser-material interaction. MRS Bull 2016;41:960–8. doi:10.1557/mrs.2016.274.
[22] Cheng J, Liu CS, Shang S, Liu D, Perrie W, Dearden G, Watkins K. A review of ultrafast laser materials micromachining. Opt Laser Technol 2013;46:88–102. doi:10.1016/j.optlastec.2012.06.037.
[23] Long J, Eliceiri M, Vangelatos Z, Rho Y, Wang L, Su Z, Xie X, Zhang Y, Grigoropoulos C. Early dynamics of cavitation bubbles generated during ns laser ablation of submerged targets. Opt Express 2020;28:14300–9. doi:10.1364/OE.391584.
[24] Nguyen TTP, Tanabe R, Ito Y. Comparative study of the expansion dynamics of laser-driven plasma and shock wave in in-air and underwater ablation regimes. Opt Laser Technol 2018;100:21–6. doi:10.1016/j.optlastec.2017.09.021.
[25] Vogel A, Busch S, Parlitz U. Shock wave emission and cavitation bubble generation by picosecond and nanosecond optical breakdown in water. J Acoust Soc Am 1996;100:148–65. doi:10.1121/1.415878.
[26] Gattass RR, Mazur E. Femtosecond laser micromachining in transparent materials. Nat Photonics 2008;2:219–25. doi:10.1038/nphoton.2008.47.
[27] Kou L, Labrie D, Chylek P. Refractive indices of water and ice in the 0.65 to 25 μm spectral range. Appl Opt 1993;32:3531. doi:10.1364/ao.32.003531.
[28] Faghri A, Zhang Y. Transport phenomena in multiphase systems. Elsevier Academic Press; 2006.
[29] E. ToolBox, Water - Thermal Diffusivity, (2018). https://www.engineeringtoolbox.com/water-steam-thermal-diffusivity-d_2058.html (accessed December 9, 2019).
[30] Rayleigh Lord. On the pressure developed in a liquid during the collapse of a spherical cavity. Philos Mag 1917;34:94–8. doi:10.1080/14786440808635681.
[31] Brennen CE. Cavitation and bubble dynamics. Cambridge University Press; 2013. doi:10.1017/CBO9781107338760.
[32] Löfstedt R, Barber BP, Putterman SJ. Toward a hydrodynamic theory of sonoluminescence. Phys Fluids A. 1992;5:2911–28. doi:10.1063/1.858700.
[33] Toegel R, Gompf B, Pecha R, Lohse D. Does water vapor prevent upscaling sonoluminescence? Phys Rev Lett 2000;85:3165–8. doi:10.1103/PhysRevLett.85.3165.
[34] Lam J, Lombard J, Dujardin C, Ledoux G, Merabia S, Amans D. Dynamical study of bubble expansion following laser ablation in liquids. Appl Phys Lett 2016;108:074104. doi:10.1063/1.4942389.
[35] Soliman W, Nakano T, Takada N, Sasaki K. Modification of Rayleigh-Plesset theory for reproducing dynamics of cavitation bubbles in liquid-phase laser ablation. Jpn J Appl Phys 2010:49. doi:10.1143/JJAP.49.116202.
[36] Çengel YA, Cimbala JM. Fluid mechanics: fundamentals and applications. McGraw-HillHigher Educ 2006.
[37] Sedov LI. Similarity and dimensional analysis in mechanics. 10th Edition. CRC Press Inc; 1993. doi:10.1016/C2013-0-08173-X.
[38] Nguyen TTP, Tanabe-Yamagishi R, Ito Y. Impact of liquid layer thickness on the dynamics of nano- to sub-microsecond phenomena of nanosecond pulsed laser ablation in liquid. Appl Surf Sci 2019;470:250–8. doi:10.1016/j.apsusc.2018.10.160.
[39] Suslick KS, Flannigan DJ. Inside a collapsing bubble: sonoluminescence and the conditions during cavitation. Annu Rev Phys Chem 2008;59:659–83. doi:10.1146/annurev.physchem.59.032607.093739.
[40] Putterman S, Evans PG, Vazquez G, Weninger K. Is there a simple theory of sonoluminescence? Nature 2001;409:782–3. doi:10.1038/35057317.
[41] Nguyen TTP, Tanabe R, Ito Y. Effects of an absorptive coating on the dynamics of underwater laser-induced shock process. Appl Phys A Mater Sci Process 2014;116:1109–17. doi:10.1007/s00339-013-8193-2.